Figure S1

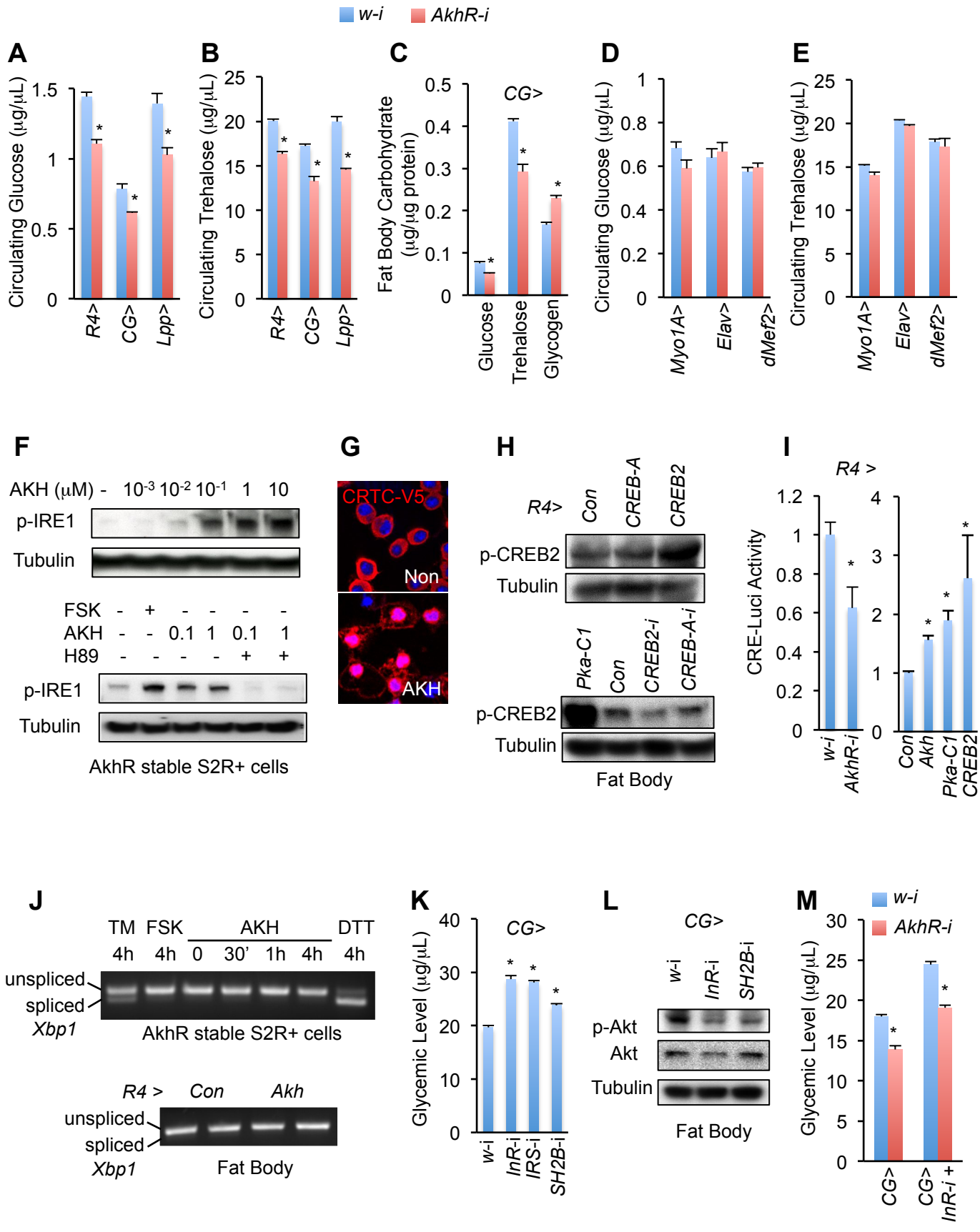
w-i
AkhR-i
A
Circulating Glucose (μg/μL)
R4>
CG>
Lpp>
B
Circulating Trehalose (μg/μL)
C
CG>
Fat Body Carbohydrate (μg/μg protein)
Glucose
Trehalose
Glycogen
D
Circulating Glucose (μg/μL)
Myo1A>
Elav>
dMef2>
E
Circulating Trehalose (μg/μL)
F
AKH (μM) - 10-3 10-2 10-1 1 10
p-IRE1
Tubulin
FSK - + - - - -
AKH - - 0.1 1 0.1 1
H89 - - - - + +
AkhR stable S2R+ cells
G
CRTC-V5
Non
AKH
H
R4> Con CREB-A CREB2
p-CREB2
Tubulin
Pka-C1 Con CREB2-i CREB-A-i
Fat Body
I
R4 >
CRE-Luci Activity
w-i
AkhR-i
Con
Akh
Pka-C1
CREB2
J
TM FSK AKH DTT
4h 4h 0 30' 1h 4h 4h
unspliced
spliced
Xbp1
AkhR stable S2R+ cells
R4 > Con Akh
unspliced
spliced
Xbp1
Fat Body
K
CG>
Glycemic Level (μg/μL)
w-i
InR-i
IRS-i
SH2B-i
L
CG>
w-i
InR-i
SH2B-i
p-Akt
Akt
Tubulin
Fat Body
M
w-i
AkhR-i
Glycemic Level (μg/μL)
CG>
CG> InR-i +

Figure S2

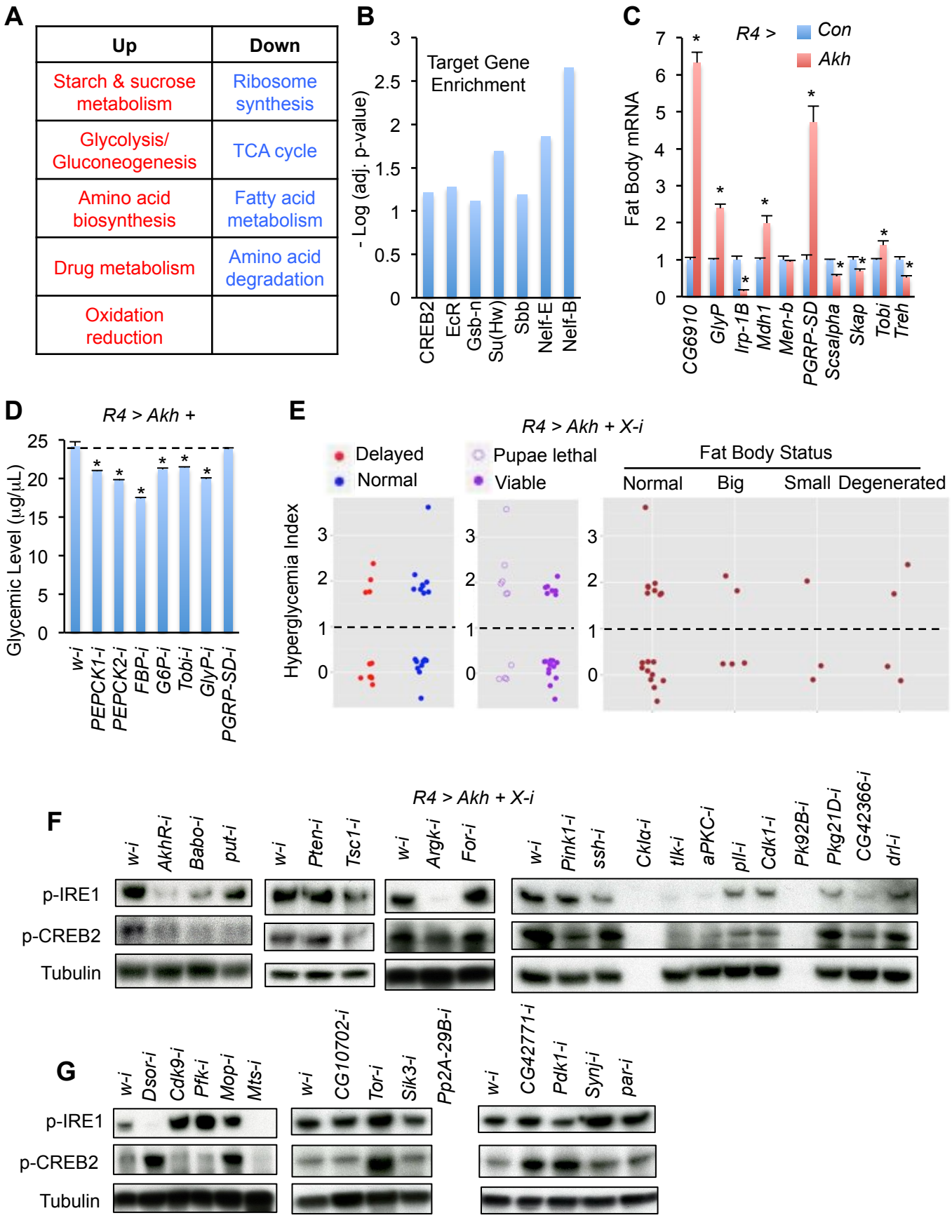
A
Up
Down
Starch & sucrose metabolism
Ribosome synthesis
Glycolysis/ Gluconeogenesis
TCA cycle
Amino acid biosynthesis
Fatty acid metabolism
Drug metabolism
Amino acid degradation
Oxidation reduction
B
Target Gene Enrichment
- Log (adj. p-value)
CREB2
EcR
Gsb-n
Su(Hw)
Sbb
Nelf-E
Nelf-B
C
R4 >
Con
Akh
Fat Body mRNA
CG6910
GlyP
Irp-1B
Mdh1
Men-b
PGRP-SD
Scsalpha
Skap
Tobi
Treh
D
R4 > Akh +
Glycemic Level (μg/μL)
w-i
PEPCK1-i
PEPCK2-i
FBP-i
G6P-i
Tobi-i
GlyP-i
PGRP-SD-i
E
R4 > Akh + X-i
Delayed
Normal
Pupae lethal
Viable
Fat Body Status
Normal
Big
Small
Degenerated
Hyperglycemia Index
F
R4 > Akh + X-i
w-i
AkhR-i
Babo-i
put-i
Pten-i
Tsc1-i
Argk-i
For-i
Pink1-i
ssh-i
Ckla-i
tlk-i
aPKC-i
pll-i
Cdk1-i
Pk92B-i
Pkg21D-i
CG42366-i
drl-i
p-IRE1
p-CREB2
Tubulin
G
Dsor-i
Cdk9-i
Pfk-i
Mop-i
Mts-i
CG10702-i
Tor-i
Sik3-i
Pp2A-29B-i
CG42771-i
Pdk1-i
Synj-i
par-i

Figure S3

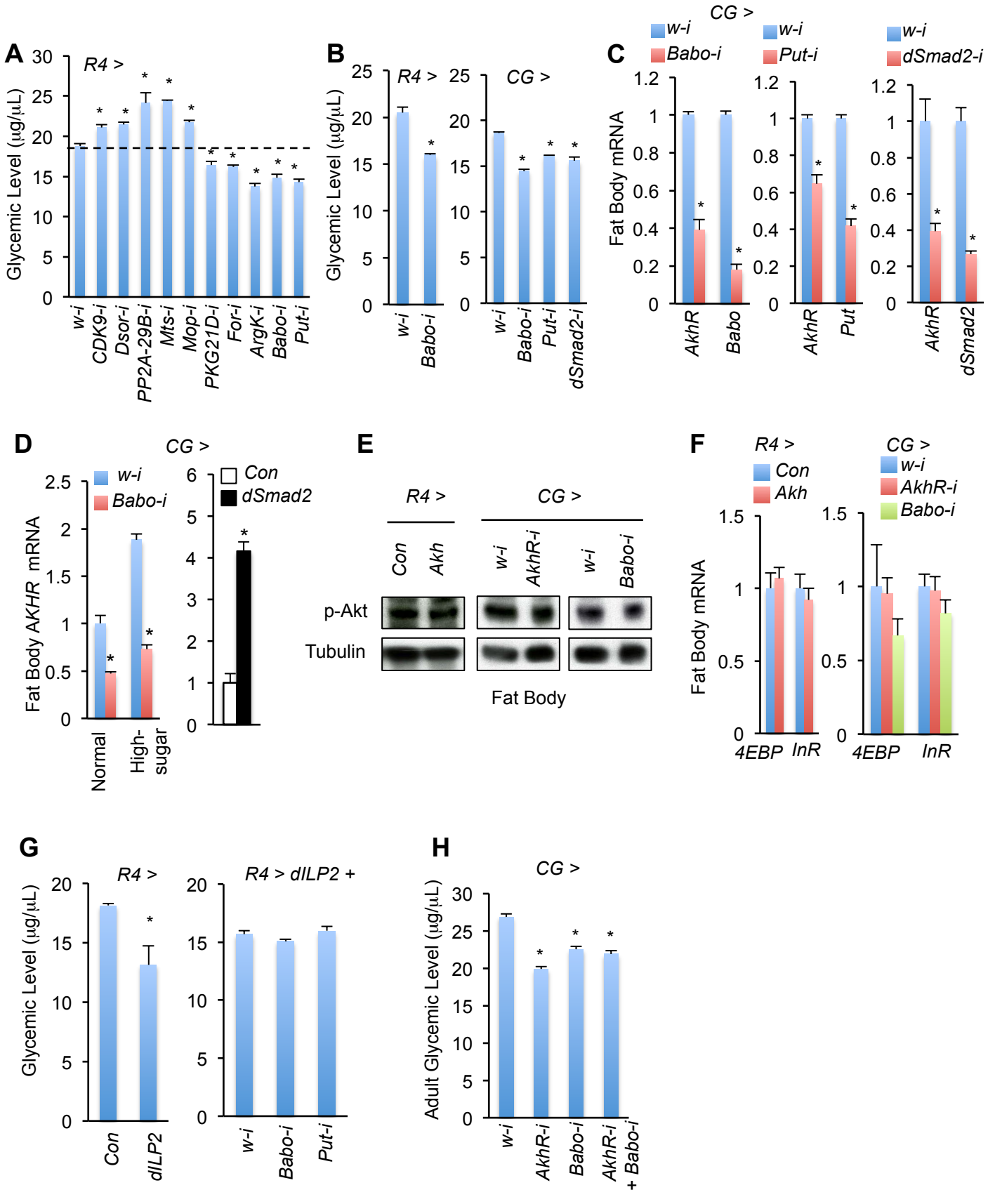
A
R4 >
Glycemic Level (μg/μL)
w-i
CDK9-i
Dsor-i
PP2A-29B-i
Mts-i
Mop-i
PKG21D-i
For-i
ArgK-i
Babo-i
Put-i
B
R4 >
CG >
Glycemic Level (μg/μL)
w-i
Babo-i
Put-i
dSmad2-i
C
CG >
w-i
Babo-i
Put-i
dSmad2-i
Fat Body mRNA
AkhR
Babo
Put
dSmad2
D
CG >
w-i
Babo-i
Con
dSmad2
Fat Body AKHR mRNA
Normal
High-sugar
E
R4 >
CG >
Con
Akh
w-i
AkhR-i
Babo-i
p-Akt
Tubulin
Fat Body
F
R4 >
CG >
Con
Akh
w-i
AkhR-i
Babo-i
Fat Body mRNA
4EBP
InR
G
R4 >
R4 > dILP2 +
Glycemic Level (μg/μL)
Con
dILP2
w-i
Babo-i
Put-i
H
CG >
Adult Glycemic Level (μg/μL)
w-i
AkhR-i
Babo-i
AkhR-i + Babo-i

Figure S4

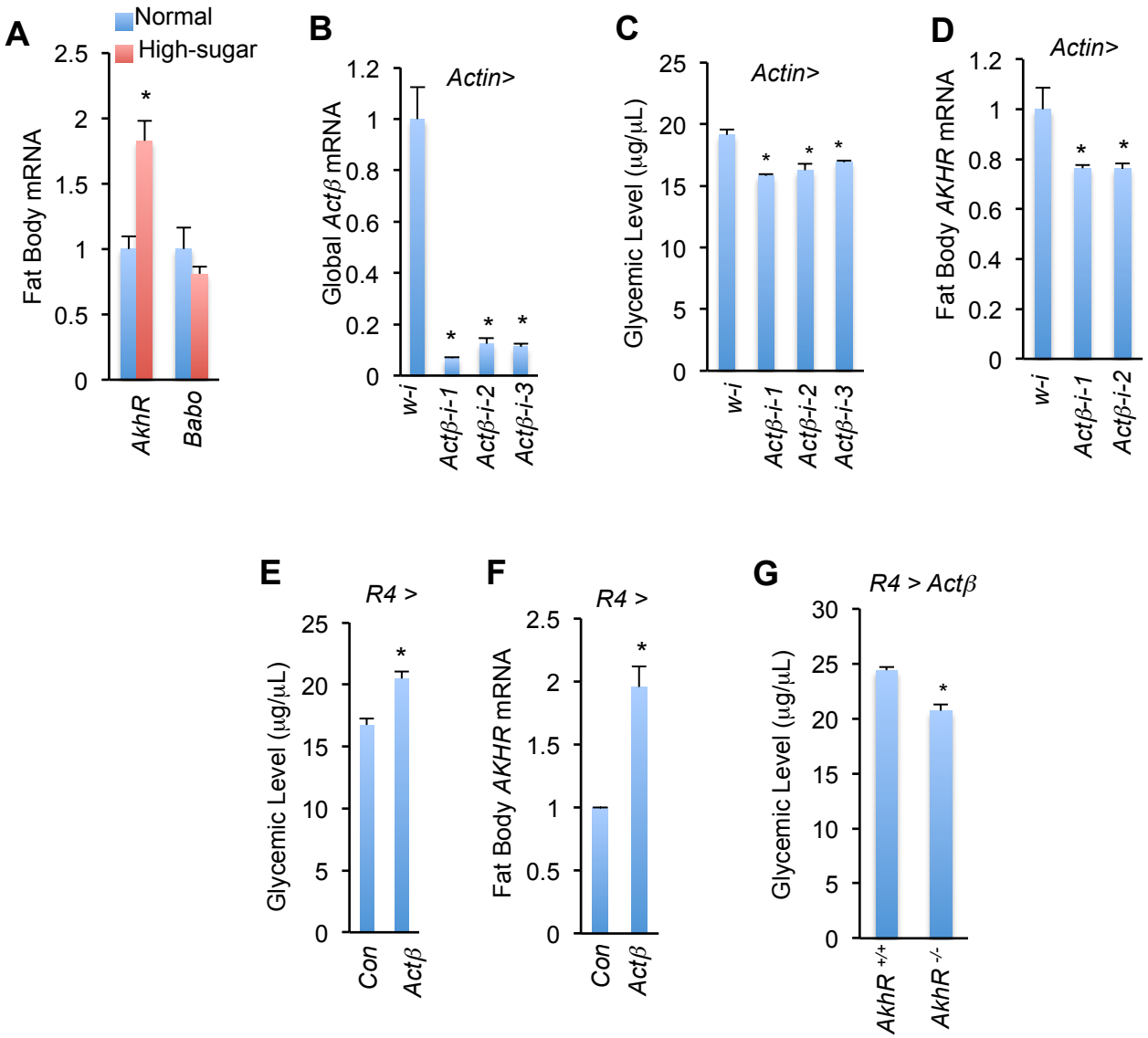
A
Normal
High-sugar
Fat Body mRNA
2.5
2
1.5
1
0.5
0
*
AkhR
Babo
B
Actin>
Global Actβ mRNA
1.2
1
0.8
0.6
0.4
0.2
0
*
*
*
w-i
Actβ-i-1
Actβ-i-2
Actβ-i-3
C
Actin>
Glycemic Level (μg/μL)
25
20
15
10
5
0
*
*
*
w-i
Actβ-i-1
Actβ-i-2
Actβ-i-3
D
Actin>
Fat Body AKHR mRNA
1.2
1
0.8
0.6
0.4
0.2
0
*
*
w-i
Actβ-i-1
Actβ-i-2
E
R4 >
Glycemic Level (μg/μL)
25
20
15
10
5
0
*
Con
Actβ
F
R4 >
Fat Body AKHR mRNA
2.5
2
1.5
1
0.5
0
*
Con
Actβ
G
R4 > Actβ
Glycemic Level (μg/μL)
30
25
20
15
10
5
0
*
AkhR +/+
AkhR -/-

Figure S5

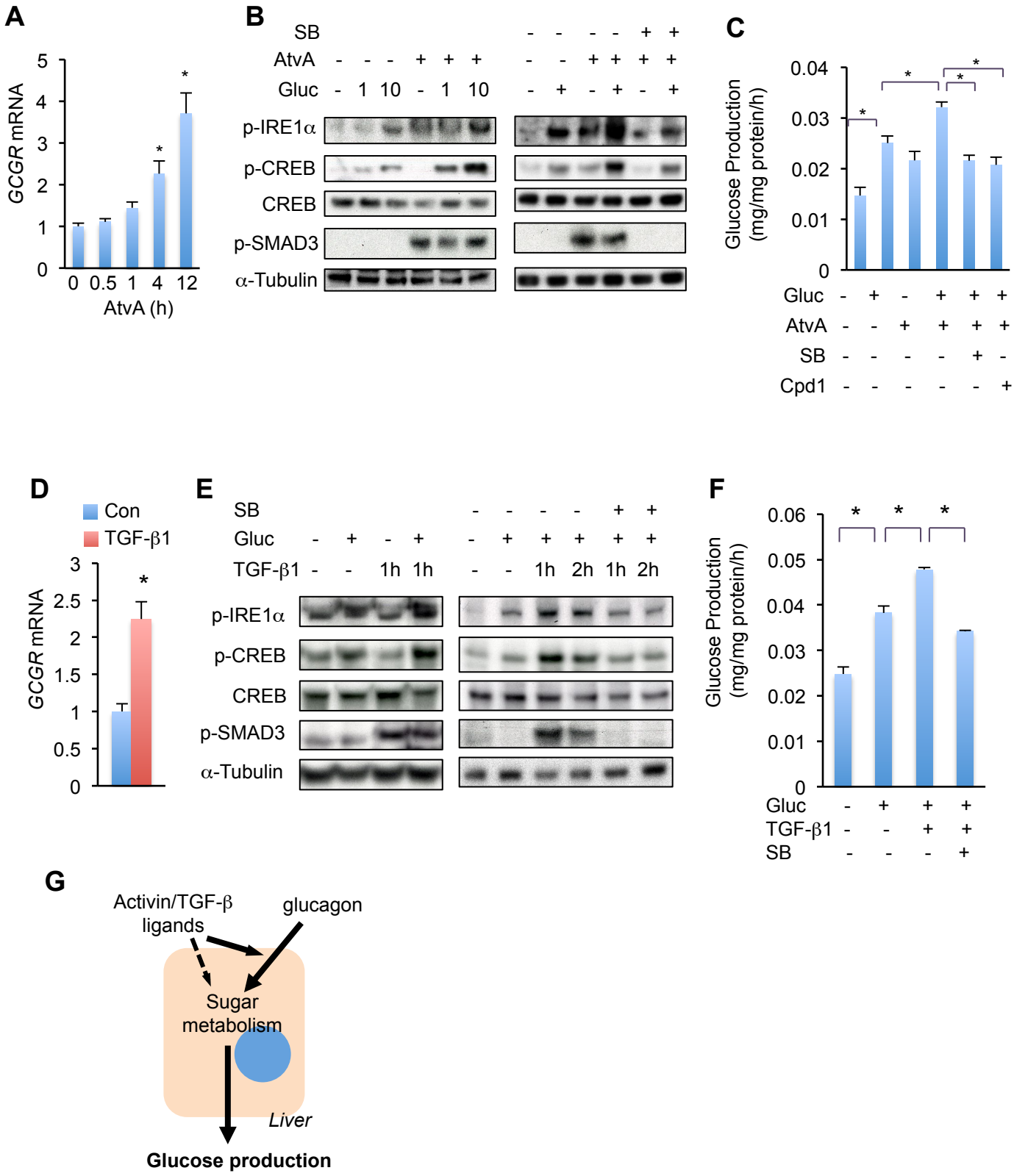
A
GCGR mRNA
AtvA (h)
0 0.5 1 4 12
B
SB
AtvA
Gluc
p-IRE1α
p-CREB
CREB
p-SMAD3
α-Tubulin
C
Glucose Production (mg/mg protein/h)
Gluc
AtvA
SB
Cpd1
D
Con
TGF-β1
GCGR mRNA
E
SB
Gluc
TGF-β1
1h 1h 1h 2h 1h 2h
p-IRE1α
p-CREB
CREB
p-SMAD3
α-Tubulin
F
Glucose Production (mg/mg protein/h)
Gluc
TGF-β1
SB
G
Activin/TGF-β ligands
glucagon
Sugar metabolism
Liver
Glucose production

Figure S6

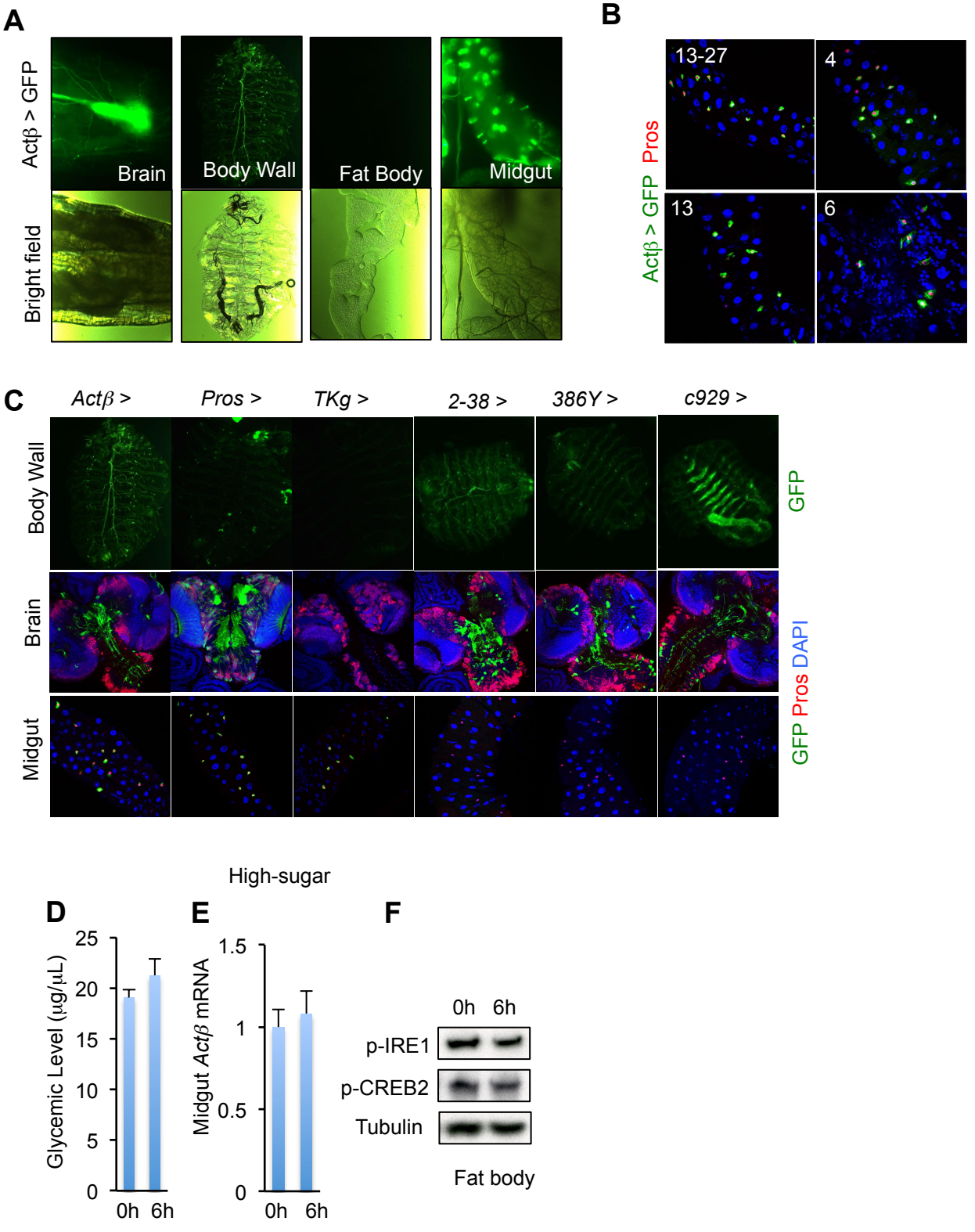
A
Actβ > GFP
Brain
Body Wall
Fat Body
Midgut
Bright field
B
13-27
4
13
6
Actβ > GFP Pros
C
Actβ >
Pros >
TKg >
2-38 >
386Y >
c929 >
Body Wall
Brain
Midgut
GFP
GFP Pros DAPI
High-sugar
D
Glycemic Level (μg/μL)
25
20
15
10
5
0
0h 6h
E
Midgut Actβ mRNA
1.5
1
0.5
0
0h 6h
F
0h 6h
p-IRE1
p-CREB2
Tubulin
Fat body

Figure S7

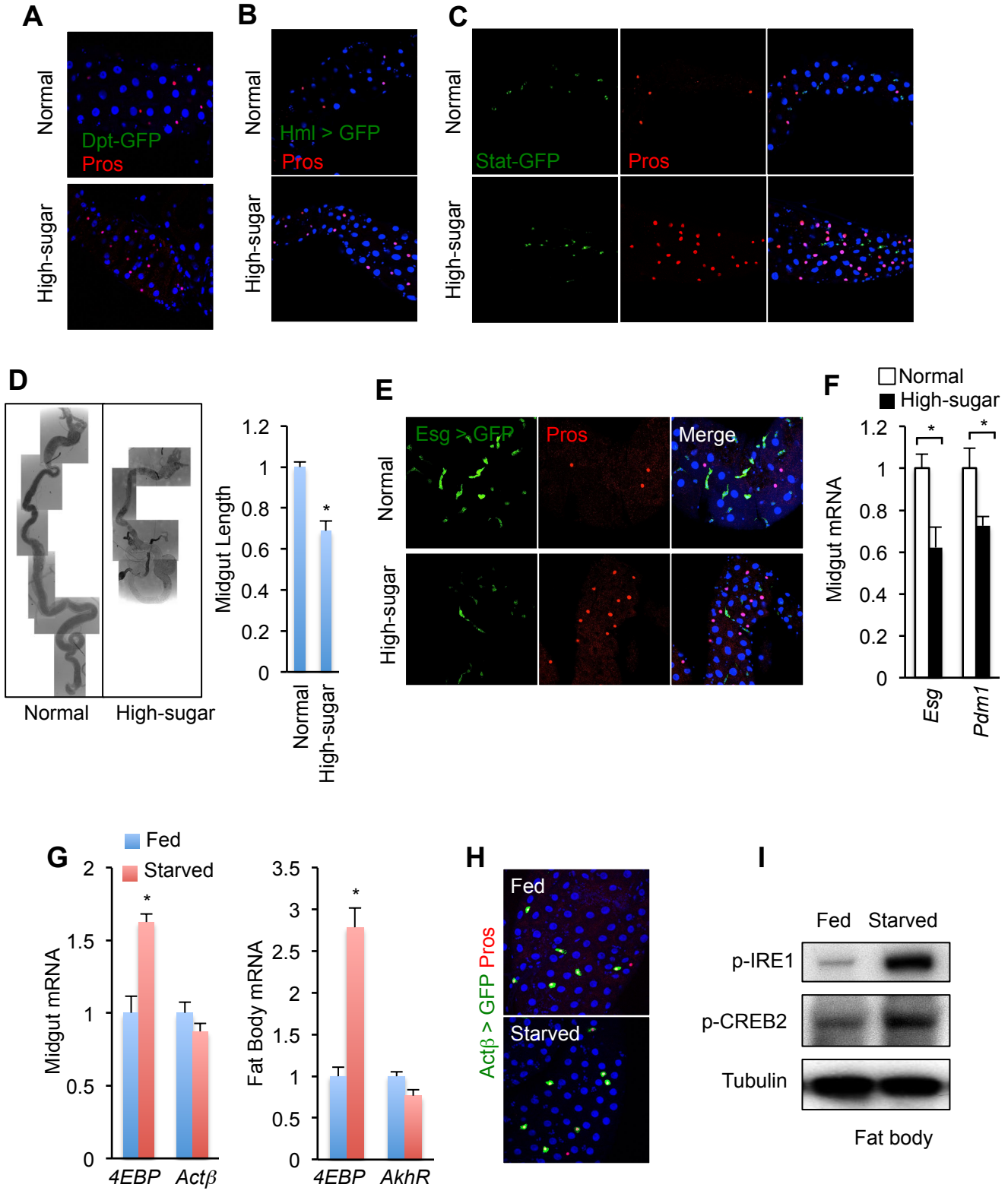
A
Normal
Dpt-GFP
Pros
High-sugar
B
Normal
Hml > GFP
Pros
High-sugar
C
Normal
Stat-GFP
Pros
High-sugar
D
Normal
High-sugar
Midgut Length
1.2
1
0.8
0.6
0.4
0.2
0
*
Normal
High-sugar
E
Esg > GFP
Pros
Merge
Normal
High-sugar
F
Normal
High-sugar
Midgut mRNA
1.2
1
0.8
0.6
0.4
0.2
0
*
*
Esg
Pdm1
G
Fed
Starved
Midgut mRNA
2
1.5
1
0.5
0
*
4EBP
Actβ
Fat Body mRNA
3.5
3
2.5
2
1.5
1
0.5
0
*
4EBP
AkhR
H
Actβ > GFP Pros
Fed
Starved
I
Fed
Starved
p-IRE1
p-CREB2
Tubulin
Fat body

Supplementary Figure and Table Legends

Figure S1, related to Figure 1. AKH signaling regulates carbohydrate metabolism. (**A-C**) Circulating glucose (**A**), circulating trehalose (**B**), and fat body stored carbohydrate levels (**C**) in 3rd instar larvae with fat body knockdown of *AkhR*. (**D-E**) Circulating glucose (**D**) and trehalose (**E**) in 3rd instar larvae with *AkhR* knockdown in different tissues (*Myo1A,* enterocytes in midgut; *Elav,* pan-neuron; *dMef2,* muscle cells) (n=4, 40 larvae). (**F**) Immunoblots of AKHR-stable S2R+ cells treated with synthetic AKH (μM) or 10 μM Forskolin (FSK, PKA agonist) for 30 min, with or without prior treatment with 10 μM H89 (PKA antagonist) for 1h. (**G**) Nuclear translocation of V5-tagged CRTC in *AkhR*-stable S2R+ cells treated with or without 1 μM AKH for 4h. (**H**) Immunoblots of p-CREB2 in larval fat bodies. (**I**) CRE-Luciferase measurements representing CREB2 transcriptional activity in larval fat bodies (n=4, 60 larval fat bodies). (**J**) IRE1 activity is not affected by AKH/PKA signaling. Spliced and unspliced *Xbp1* transcripts detected by PCR in *AkhR*-overexpressing S2R+ cells that were treated with 10 μg/mL tunicamycin (TM), 10 μM Forskolin (FSK), 10 μM AKH, or 5 mM DTT for the indicated times (up) and in 3rd instar larval fat bodies overexpressing *AKH* (down). (**K, L**) Glycemic levels (**K**) (n=4, 40 larvae) and insulin signaling in fat body (**L**, indicated by p-AKT) in 3rd larvae with knockdown of insulin signaling components. (**M**) Glycemic levels in 3rd larvae with knockdown of *AkhR, InR,* or both in fat bodies (n=4, 40 larvae). Data are presented as means ± SEM. * $p < 0.05$.

Figure S2, related to Figure 2. Large-scale RNAi screen in hyperglycemic *R4 > Akh* flies. (**A**, **B**) GO enrichment (**A**) and transcriptional factor target gene enrichment (**B**) of differentially expressed genes in AKH-expressing larval fat bodies. (**C**) Carbohydrate metabolic genes were validated by qPCR (n=4, 40 larvae). (**D**) Knockdown of certain carbohydrate metabolic genes in fat body alleviated AKH-induced hyperglycemia (n=4, 40 larvae). (**E**) No strong correlation was observed between glycemic effects and fat body status, developmental

delay, or pupal lethality associated with candidate gene knockdown. *AkhR-i* did not affect developmental delay, pupal lethality, or fat body status as compared to *w-i*. In each knockdown genotype, fat body protein level that was increased or decreased by > 40% was defined as “big” or “small” accordingly, while fat body that was degenerated and hard to collect was defined as “degenerated”. > 70% failed to emerge to adult flies were defined as “pupae lethality”. Larval development into pupa that was delayed by > 24h was defined as “developmental delay”. (**F, G**) Immunoblots of p-IRE1 and p-CREB2 in the 3rd instar larval fat bodies with AKH overexpression and candidate gene knockdown. Gene knockdowns are associated with suppressed (**F**) or enhanced (**G**) hyperglycemia. Note that knockdown of *CkI*α, *Pk92B*, *mts*, or *Pp2A-29B* causes fat body degeneration in *R4 > Akh* larvae and makes it difficult to evaluate AKH signaling regulation. Data are presented as means ± SEM. * $p < 0.05$.

Figure S3, related to Figure 3. Babo signaling regulates AKH signaling and glycemic level. (**A**) Knockdown of several candidates from the RNAi screen in wild type larval fat body also affects glycemic levels (n=4, 40 larvae). (**B**) Knockdown of Babo signaling components reduced glycemic levels in wild type 3rd instar larvae (n=4, 40 larvae). (**C**) *AkhR* mRNA levels in 3rd instar larval fat bodies with knockdown of indicated Babo signaling components (n=4, 40 larval fat bodies). (**D**) *AkhR* mRNA levels in *Babo* knockdown (left) or *dSmad2* overexpression (right) larval fat bodies (n=4, 40 larval fat bodies). (**E**) Immunoblots of p-AKT, indicative of insulin signaling, in 3rd instar larval fat bodies. (**F**) qPCR results of mRNA levels of two FoxO target genes, *InR* and *4EBP*, in 3rd instar larval fat bodies (n=4, 40 larval fat bodies). (**G**) Glycemic levels in 3rd instar larvae with fat body overexpression of *dILP2* and knockdown of *Babo* or *Put* (n=4, 40 larvae). (**H**) Glycemic levels of 5d old adult flies with fat body knockdown of *AkhR, Babo,* or both (n=4, 120 adult flies). Data are presented as means ± SEM. * $p < 0.05$.

Figure S4, related to Figure 4. Actβ regulates glycemic levels in an AkhR-dependent manner. (**A**) mRNA expression levels in the fat body (n=4, 40 larval fat bodies). (**B-D**) Global *Actβ* mRNA levels (**B**, n=4, 40 larvae), glycemic levels (**C**, n=4, 40 larvae), as well as fat body *AkhR* mRNA levels (**D**, n=4, 40 larval fat bodies), in *Actin* > *Actβ-i* 3rd instar larvae (*Actβ*-i-1, RNAi line JF03276 from TRiP. *Actβ* -i-2 and -3, RNAi lines 11062R-1 and 11062R-2 from NIG, respectively). (**E, F**) Glycemic level (**E**) and fat body *AkhR* mRNA level (**F**) in *R4* > *Actβ* 3rd instar larvae. (**G**) Glycemic levels in 3rd instar larvae with indicated genotypes (*R4-Gal4/UAS-Actβ V.S. AkhR⁻/AkhR⁻; R4-Gal4/UAS-Actβ*). Data are presented as means ± SEM. * $p < 0.05$.

Figure S5, related to Figure 4. Activin/TGF-β1 signaling promotes glucagon action in primary mouse hepatocytes. (**A**) mRNA levels of *glucagon receptor* (*GCGR*) in primary mouse hepatocytes treated with 100 ng/mL Activin A (ActA) (n=4). (**B**) Immunoblots in hepatocytes treated with 100 ng/mL AtvA and 10nM SB-431542 (SB), activin type I receptor inhibitor, prior to glucagon stimulation (Gluc, 1 or 10 nM (left) or 10 nM (right)). (**C**) Glucose productions in primary mouse hepatocytes treated with 100 ng/mL AtvA, 10 nM SB, or 10 μM Cpd1 for 4h prior to treatment with 10 nM glucagon for 4h (n=4). (**D**) mRNA levels of *glucagon receptor* (*GCGR*) in primary mouse hepatocytes treated with 10 ng/mL TGF-β1 for 1h (n=4). (**E**) Immunoblots of p-IRE1α and p-CREB in hepatocytes treated with 10 ng/mL TGF-β1 and 10nM SB for 1h or 2h prior to glucagon stimulation (Gluc, 10 nM). (**F**) Glucose production in primary mouse hepatocytes (h) treated with 10 ng/mL TGF-β1 or 10 nM SB for 1h prior treatment with 10 nM glucagon for 4h (n=4). (**G**) Model of the regulation of AKH/glucagon action and glycemic levels by activin signaling. Data are presented as means ± SEM. * $p < 0.05$.

Figure S6, related to Figure 6. Actβ expression pattern in 3rd instar larva. (**A**) *Actβ > GFP* expression (green) in 3rd instar larval brain, body wall, and midgut, but not in fat body. (**B**) GFP (green) indicates that independent Actβ-Gal4 lines express in EEs, labeled with Pros (red). (**C**) Expression patterns of different Gal4 line-driving GFP in body wall, brain, or midgut. (**D-F**) Glycemic level (**D**) (n=4, 40 larvae), midgut Actβ mRNA expression indicated by qPCR (**E**) (n=4, 40 larval midguts), and fat body immunoblots (**F**) in 3rd instar larvae fed with high-sugar diet for 6h. Data are presented as means ± SEM. * $p < 0.05$.

Figure S7, related to Figure 7. Chronic high-sugar feeding increases Actβ EE cell number. (**A-C**) *Dpt-GFP* reporter (**A**), *Hml > GFP* expression (**B**), and *10XSTAT-GFP* reporter (**C**) in 3rd instar larval midgut fed with normal or high-sugar diet through development. *Dpt-GFP* represents Relish signaling activity, and *Hml > GFP* labels hemocytes. These reporters are not expressed in the larval midgut under either normal or high-sugar diet. The *10XSTAT-GFP* reporter, indicating JAK/STAT signaling, is only expressed in small cells other than EEs in the midgut. (**D**) Image (left) and length (right) of 3rd instar larval midgut under a chronic high-sugar diet. (**E-F**) Cell morphology (**E**) and gene expression (**F**) in the larval midgut under a chronic high-sugar diet (n=4, 40 midguts). (**G-I**) Gene expression in the midgut (left) and fat body (right) (**G**), Actβ-positive cells (green) and EEs (red) in the midgut (**H**), and phosphorylation of IRE1 and CREB2 in the fat body (**I**) of 3rd instar larvae with or without 6h starvation. Data are presented as means ± SEM. * $p < 0.05$.

Table S1, related to Figure 2. RNA-seq analysis of differentially expressed genes in 3rd instar larval fat body.

Table S2, related to Figure 2. Novel hits in AKH action regulation from the *in vivo* RNAi screen. Glycemic levels were normalized to both *AkhR*-i and *w*-i

that were set as “0” and “1” (100%) hyperglycemia, respectively. RNAi hits that significantly affect hyperglycemia (< 0.3 or > 1.7) were considered as significant regulators.

Supplementary Methods

Drosophila strains.

Flies were maintained at 25°C on a 12h light, 12h dark light cycle. Flies were raised on a standard cornmeal/agar diet (10 g/L agar, 230 g/L soy flour, 30 g/L yeast, 100 g/L cornmeal, 74 g/L molasses, 4.5 g/L propionate, and 6 g/L Nipogen). All experiments were performed using 3rd instar stage larvae (12~24h before wandering). *CG-Gal4*, *R4-Gal4*, and *Lpp-Gal4* were used to target the larval fat body. *CG-* and *R4-Gal4* are stronger than Lpp-Gal4 and therefore were used for most assays in this study. Fat body genetic manipulation using *CG-* or *R4-Gal4* results in the same changes in both physiology and signaling, except that *CG-Gal4/UAS-Akh* causes lethality. The genotype of *AKH* overexpressing flies is *UAS-Akh; R4-Gal4 / T(2;3)B3, CyO: TM6B, Tb.* Fat body overexpression of *Actβ* or *Daw* (CG- or R4-Gal4) causes sterility or adult lethality, we therefore performed genetic manipulations in fat body-expressing *Actβ* or *Daw* flies by crossing UAS lines to *Cg-Gal4, tub-Gal80^{ts}; UAS-Actβ* or *Cg-Gal4, tub-Gal80^{ts}; UAS-Daw* flies at 18°C and culturing offspring larvae at 29°C until they reached the 3rd instar larval stage.

The following Gal4 driver lines were used to target various cells/tissues: *CG-Gal4 (*BLM 7011), *R4-Gal4 (*BLM 33832) and *Lpp-Gal4* (fat body) (Palm et al., 2012), *dMef2-Gal4* (muscle) (Owusu-Ansah et al., 2013), *Myo1A-Gal4* (midgut) (Amcheslavsky et al., 2014; Song et al., 2014), *Elav-Gal4* (pan-neuron) (Song et al., 2014), *TKg-Gal4* (TK EE) (Amcheslavsky et al., 2014; Song et al., 2014), *386Y-Gal4 and c929-Gal4* (neuroendocrine cell) (Marques et al., 2003), *Hml-Gal4* (BLM 30140) (hemocytes). *Pros-Gal4* (peripheral neuron, a kind gift from Allison Bardin) and *2-38-Gal4* (EE, a kind gift from Katja Brückner) were previously described (Hang et al., 2014; Makhijani et al., 2011). *Actβ-Gal4-4* was from the HHMI Janelia Research Campus (BLM 49078). Other *Actβ-Gal4* lines, including -6, -13, and -13+27, were created by using sense primer 5'-GGCAATGGACGACGGAAGCAGTTTAC-3' and antisense primer 5'-GGCAAGCGTGTAGTACAGGCACTGT-3' to amplify a 5.6 kb *Drosophila* Actβ promoter/enhancer. The region was initially cloned in a PCRII TOPO vector (Invitrogen) before it was transferred to the pPelican-Gal4 vector that bears insulation DNA sequences (Barolo et al., 2000). These four *Actβ-Gal4* lines exhibited very similar expression patterns in 3rd instar larvae.

Fly stocks with RNAi transgenes targeting *white* (JF01545), *Akh* (HMS00477), *AkhR* (JF03256), *InR* (JF01482), *Ire1* (HMS03003), *Creb2* (JF02494), *Crtc* (HM05069), *Sik3* (JF03002), *Babo* (JF01953), *Put* (HMS01944), *Sax* (JF03431), *Tkv* (JF01485), *dSmad2* (JF02320), *Mad* (JF01263), *Daw* (HMS01110), *Actβ* (JF03276), *Chico/IRS* (JF02964), *CerbA* (JF02189), *Pten* (HMS00044), *Tsc1* (JF01484), *Cdk9* (HMS01391), *Dsor1* (JF03100), *Pp2A-29B* (JF03316), *Mts*

(JF02805), *Mop* (HMS00706), *Pkg21D* (JF02766), *For* (JF01181), and *ArgK* (JF02699) were obtained from the TRiP at Harvard Medical School (http://www.flyrnai.org/TRiP-HOME.html). RNAi fly stocks targeting *Actβ* (11062R-1 and 11062R-2) were obtained from the NIG-FLY stock center (www.shigen.nig.ac.jp/fly/nigfly), and *SH2B* (32892 and 103646) were obtained from the VDRC (stockcenter.vdrc.at). RNAi fly stocks targeting *CBP* (BLM 32576) and specific *Babo* isoforms (a, BLM 44400; b, BLM 44401; c, BLM 44402) (Awasaki et al., 2011) were obtained from the Bloomington *Drosophila* Stock Center (flystocks.bio.indiana.edu). Multiple RNAi fly stocks were used to confirm the knockdown effect and the most significant ones are listed here.

The overexpression and other fly stocks, including *UAS-Akh* (BLM 27343), *UAS-Pka-C1* (BLM 35555), *UAS-Creb2* (BLM 9232), *UAS-CrebA* (BLM 32572), *UAS-Babo*, *UAS-dSmad2*, *UAS-Actβ*, *UAS-Daw,* actβ^{ed80} mutant, *UAS-dILP2*, *CRE-Luci,* and *10XSTAT-GFP* were previously described (Bach et al., 2007; Ghosh and O'Connor, 2014; Gibbens et al., 2011; Rajan and Perrimon, 2012; Song et al., 2014; Zhu et al., 2008). *AkhR* null mutant (a kind gift from Ronald Kühnlein) and *Dpt-GFP* (a kind gift from Paula I. Watnick) were previously described (Gronke et al., 2007; Siudeja et al., 2015).

High-sugar diet and carbohydrate measurement.

25% extra sucrose was added into the standard diet to generate the high-sugar diet food. For chronic high-sugar feeding, the parental females were allowed to lay eggs on high-sugar food media, such that larvae were cultured on high-sugar

food throughout development. For acute high-sugar feeding, late 3rd instar larvae were transferred to a high-sugar diet for 6h. The method we used to determine circulating trehalose levels has previously been described (Song et al., 2010). Briefly, 2 μL hemolymph from 3rd instar larvae or 5d old adult flies was diluted in 38 μL sugar buffer (5 mM Tris [pH 6.6], 137 mM NaCl, 2.7 mM KCl) and heated at 70°C to inactivate endogenous trehalase activity. After a brief centrifugation, 10 μL supernatant was treated with 0.2 μL water or trehalase (Megazyme, E-TREH) at 37°C for 20 min to digest trehalose into glucose, then glucose levels were measured by incubation with 150 μL glucose assay reagent (Megazyme) at 37°C for 5 min. The absorbance at 510 nm was measured on a Molecular Devices SpectraMax Paradigm plate reader. Circulating trehalose levels were determined by subtracting circulating free glucose levels from total glucose levels after enzyme digestion. We defined circulating trehalose + glucose as the 'glycemic level' in this study.

Measurement of carbohydrates stored in the larval fat body has been previously described (Song et al., 2010). Briefly, 10 3rd larval fat bodies were homogenized in 300 μL PBS containing 0.1% Triton-X and protease inhibitor and heated at 70°C for 5 min to inactivate endogenous enzymes. After centrifugation at 13,000 rpm for 10 min at 4°C, 10 μL supernatant of lysate was treated with 0.2 μL trehalase (Megazyme, for trehalose measurement) or 1 μL amyloglucosidase (Sigma, for glycogen measurement) at 37°C for 20 min, and glucose levels were measured using a glucose assay reagent (Megazyme). 10 μL supernatant was used for protein level measurement using the Bradford reagent (Sigma). A

relative level of trehalose or glycogen was determined by subtracting free glucose levels from total glucose levels after enzyme digestion and then normalized to protein levels.

Generation of stable AkhR-expressing S2R+ cells. A full-length *AkhR* cDNA was generated by RT-PCR using primers 5'-CCGGAATTCGAGGCAAATCCTTGATGCAG and 5'-AGAATGCGGCCGCACTTCTGGCGGATCGGGGAT, verified by DNA sequencing, and inserted into the plasmid vector pAC5-Stable2-Puro, which allows for multicistronic expression of the target protein and GFP as well as a protein conferring puromycin resistance (Gonzalez et al., 2011). S2R+ cell transfection was performed using the non-liposomal reagent Effectene (Qiagen) following the manufacturer's instructions. 72 hours after transfection, cells were incubated for two weeks in selective medium, i.e. Schneider's medium (Invitrogen) containing 10% FBS, standard cell culture antibiotics, and 10 μg/mL puromycin. Cells were split as necessary and again incubated in selective medium. Stable cells were maintained with selective medium and AKH treatment performed in medium without puromycin.

qPCR

10 fat bodies, 10 midguts, 10 body walls, or 10 brains from late 3rd instar larvae of each genotype were collected on ice and stored at -80°C. Total RNA from fat

bodies or mouse primary hepatocytes were extracted using Trizol (Invitrogen) and cDNA transcribed using the iScript cDNA Synthesis Kit (Biorad). qPCR was then performed using iQ SYBR Green Supermix on a CFX96 Real-Time System/C1000 Thermal Cycler (Biorad). *Drosophila* and mouse gene expression were normalized to *RpL32* and *β-actin*, respectively. Primers are listed as below:

Drosophila

RpL32-F:	GCTAAGCTGTCGCACAAATG
RpL32-R:	GTTCGATCCGTAACCGATGT
AkhR-F:	GCTATCCACGGACCTGATGTG
AkhR-R:	CTGTCGAGCGATATGCAGACC
Actβ-F:	ACGGCAAATTTTGACAAAGC
Actβ-R:	TTGGTATCATTCGTCCACCA
Babo-F:	GCTGGCCGCTGATAACAGAA
Babo-R:	AGGCTGAGCAATGTAGATGGG
Put-F:	TTTTGCCCGGAAGTCATGGG
Put-R:	TGCTCTATCCGTGTTTCACATTG
dSmad2-F:	CCGACTCCATTGTGGACTATCC
dSmad2-R:	CCCAATTCCATGTACTGCGG
Pros-F:	TTTGACCGGAGATGGTGACG
Pros-R:	GGTCGTTCCTGCCCAGTTTC
Esg-F:	ATGAGCCGCAGGATTTGTG
Esg-R:	CCTCCTCGATGTGTTCATCATCT
Pdm1:	AGCTGTCCTAACGAGTTCCG

Pdm1:	ACATCGCGCATATTTGTGTCAA
CG6910-F:	CCGGGACTACAGTATGGACAC
CG6910-R:	CGAAATCCACAGTCTGGTTCAG
GlyP-F:	GCTCACTGACCAACACCATGA
GlyP-R:	AACGGATGCCATAGCCATAGG
Irp-1B-F:	TCGCCCAGTTCGAGAAAACTT
Irp-1B-R:	GGATCGAGTAGGGCAGTTGA
Mdh1-F:	CTCGGCTATGACTCGCCTG
Mdh1-R:	CTTAACAGCAGAAATTGGCACAC
Men-b-F:	GCGCTTCAAGACGCAAGAG
Meb-b-R:	CGTACAGATCGCTCAGATAGAGA
PGRP-SD-F:	GACAGCATGGAAACTCCCTTG
PGRP-SD-R:	GTTTTGCAGATTTTGCATGTGC
Scsalpha-F:	CGGAACCGACTTCATCGACTG
Scsalpha-R:	CCTTGATGCCCGAATTGTACTC
Skap-F:	CCCCTGATCGAAACCGTTAGG
Skap-R:	GGAAACGTGTTCCTGGACATT
Tobi-F:	GTCATGCATCCTGTGTGGTC
Tobi-R:	GATTTCCAGCTGGCTGTTGT
Treh-F:	GGCACCGAGCTTGAGAAATG
Treh-R:	ATTTTGCGTCCCAAGTCCTTC
Mouse	
β-actin-F:	AGTGTGACGTTGACATCCGTA

β-actin-R: GCCAGAGCAGTAATCTCCTTCT

GCGR-F: TTGCTGGTTGCTGGTAGAGG

GCGR-R: AGGGGATGACAAACAGCAGG

CREB transcriptional activity and IRE1 nuclease activity. 15 larval fat bodies that carry *CRE-Luci* were isolated and homogenized in 150 μL PBS containing 0.1% Triton-X and protease inhibitor. After centrifugation at 13,000 rpm for 10 min at 4°C, 50 μL lysate was collected for luciferase activity measurement using a Luciferase Assay Kit (Promega). 10 μL lysate was incubated with 200 μL Bradford reagent (Sigma) for protein quantification. CREB transcriptional activity was then determined by normalizing CRE-Luciferase activity to protein levels. IRE1 nuclease activity was measured by monitoring *Xbp1* mRNA splicing as previously described (Plongthongkum et al., 2007). Briefly, total RNA from S2R+ cells or from fat bodies was extracted and transcribed into cDNA. Spliced and unspliced *Xbp1* mRNAs were detected by PCR using primer pairs that flank the intron. Xbp1-F: CCGAATTCAAGCAGCAACAGCA and Xbp1-R: TAGTCTAGACAGAGGGCCACAATTTCCAG.

RNA-seq transcriptome analysis. 10 fat bodies from late 3rd instar larvae of each genotype were collected on ice and stored at -80°C. Total RNA was extracted using Trizol (Invitrogen). To prepare RNA samples for RNA-seq, RNA integrity (> 6.5) was assessed using an Agilent Bioanalyzer. Sequencing libraries

were constructed using Illumina Hi-seq kits following standard protocol, and 100 bp pair end reads were generated at Novogene Bioinformatics Institute (Beijing, China). Sequence reads were mapped back to the *Drosophila* genome (FlyBase genome annotation version r5.51) using TopHat. Using uniquely mapped reads, gene expression levels were quantified using Cufflinks (FPKM values). Next, we performed data normalization on the read counts and applied a negative binomial statistical framework using the Bioconductor package DESeq to quantify differential expression between experimental and control data. Differentially expressed genes were selected if 2 or more fold changes were consistently observed among replicates. Genes with less than 2 but greater than 1.5 fold changes and with an adjusted p-value of 0.05 or better were also selected. For gene list enrichment analysis, we assembled gene lists, including pathways, complexes and transcription factor target gene sets, from various public resources including Gene Ontology (GO), KEGG, DroID, and other published datasets. CREB2 target genes were predicted based on the presence of a cAMP-responsive element (CRE) “TGG/ACGTCA” in the promoter region. Enrichment p-values were calculated using hyper-geometric distribution, and gene lists with an enrichment p-value of less than 0.05 were presented.

Primary hepatocyte culture, HGP assays and immunoblots. Mouse primary hepatocytes were prepared by liver perfusion with type II collagenase (Worthington Biochemical, Lakewood, NJ) and grown at 37°C on collagen-coated

plates to be treated with the desired reagents. HGP assays were previously described (Mao et al., 2011; Sheng et al., 2012). Briefly, after treatment with different reagents (see below), hepatocytes were incubated for 4h in glucose-free DMEM (Sigma) supplemented with 20 mM sodium lactate, 1 mM sodium pyruvate, 2 mM L-glutamine, and 15 mM HEPES, without phenol red. Glucose levels in the culture medium were measured using a glucose assay reagent (Megazyme, K-GLUC) and normalized to hepatocyte protein levels measured with the Bradford reagent (Sigma). Immunoblotting was done as previously described (Song et al., 2010; Song et al., 2014). Briefly, fat bodies dissected from late 3rd instar larvae or AKHR-expressing S2R+ cells were incubated in serum-free Schneider's *Drosophila* media (Invitrogen) with or without synthetic AKH or other reagents at room temperature to modulate AKH signaling. Fat bodies, S2R+cells, and primary hepatocytes were lysed in buffer (50 mM Tris-HCl [pH 7.5], 5 mM EDTA, 10 mM Na4P2O7, 100 mM NaF, 1 mM phenylmethylsulfonyl fluoride, 1 mM Na3VO4, 10 μg/ml aprotinin, 10 μg/ml leupeptin, 1% Nonidet P-40). Rabbit anti-phospho-CREB for mouse p-CREB (1:1000, Cell Signaling), rabbit anti-phospho-IRE1α for mouse p-IRE1α and *Drosophila* p-IRE1 (1:1000, Abcam), rabbit anti-phospho-PKA-substrate for *Drosophila* p-CREB2 (1:1000, Cell Signaling), rabbit anti-phospho-SMAD3 for mouse p-SMAD3 (1:1000, Abcam), rabbit anti-CREB for mouse CREB (1:1000, Cell Signaling) and mouse anti-α-Tubulin for mouse α-Tubulin and *Drosophila* Tubulin (1:5000, Sigma). The following chemicals were used for *in vitro* treatment in this study: synthetic *Drosophila* AKH (pQLTFSPDWa, NeoBioLab) (Park et al., 2002), glucagon

(Sigma), Activin A (R&D), TGF-β1 (Novoprotein), Myostatin (R&D), Forskolin (Abcam), H89 (Sigma), SB 431542 (Abcam), and Cpd1 (Santa Cruz).

Immunostaining. Immunostainings of S2R+ cells and larval midgut and brain were described previously (Song et al., 2010; Song et al., 2014). Samples were fixed for 15 min in 4% formaldehyde/PBS. After fixation samples were washed with PBS containing 0.2% Triton-X and incubated with primary antibodies overnight at 4°C. Next, the samples were incubated with secondary antibodies (1:500) and DAPI (1:1000) for 1h at room temperature, washed and mounted in Vectashield (Vector). Primary antibodies used in this study were: rabbit anti-Tachykinin (1:1000) (Song et al., 2014), mouse anti-Prospero (DSHB, 1:100), and mouse V5 (1:1000, ThermoFisher). Confocal images were obtained using a Leica TCS SP2 AOBS system.

References

Amcheslavsky, A., Song, W., Li, Q., Nie, Y., Bragatto, I., Ferrandon, D., Perrimon, N., and Ip, Y.T. (2014). Enteroendocrine cells support intestinal stem-cell-mediated homeostasis in Drosophila. Cell Rep *9*, 32-39.

Awasaki, T., Huang, Y., O'Connor, M.B., and Lee, T. (2011). Glia instruct developmental neuronal remodeling through TGF-beta signaling. Nat Neurosci *14*, 821-823.

Bach, E.A., Ekas, L.A., Ayala-Camargo, A., Flaherty, M.S., Lee, H., Perrimon, N., and Baeg, G.H. (2007). GFP reporters detect the activation of the Drosophila JAK/STAT pathway in vivo. Gene Expr Patterns *7*, 323-331.

Barolo, S., Walker, R.G., Polyanovsky, A.D., Freschi, G., Keil, T., and Posakony, J.W. (2000). A notch-independent activity of suppressor of hairless is required for normal mechanoreceptor physiology. Cell *103*, 957-969.
Ghosh, A.C., and O'Connor, M.B. (2014). Systemic Activin signaling independently regulates sugar homeostasis, cellular metabolism, and pH balance in Drosophila melanogaster. Proc Natl Acad Sci U S A *111*, 5729-5734.
Gibbens, Y.Y., Warren, J.T., Gilbert, L.I., and O'Connor, M.B. (2011). Neuroendocrine regulation of Drosophila metamorphosis requires TGFbeta/Activin signaling. Development *138*, 2693-2703.
Gonzalez, M., Martin-Ruiz, I., Jimenez, S., Pirone, L., Barrio, R., and Sutherland, J.D. (2011). Generation of stable Drosophila cell lines using multicistronic vectors. Sci Rep *1*, 75.
Gronke, S., Muller, G., Hirsch, J., Fellert, S., Andreou, A., Haase, T., Jackle, H., and Kuhnlein, R.P. (2007). Dual lipolytic control of body fat storage and mobilization in Drosophila. PLoS Biol *5*, e137.
Hang, S., Purdy, A.E., Robins, W.P., Wang, Z., Mandal, M., Chang, S., Mekalanos, J.J., and Watnick, P.I. (2014). The acetate switch of an intestinal pathogen disrupts host insulin signaling and lipid metabolism. Cell Host Microbe *16*, 592-604.
Makhijani, K., Alexander, B., Tanaka, T., Rulifson, E., and Bruckner, K. (2011). The peripheral nervous system supports blood cell homing and survival in the Drosophila larva. Development *138*, 5379-5391.
Mao, T., Shao, M., Qiu, Y., Huang, J., Zhang, Y., Song, B., Wang, Q., Jiang, L., Liu, Y., Han, J.D.*, et al.* (2011). PKA phosphorylation couples hepatic inositol-requiring enzyme 1alpha to glucagon signaling in glucose metabolism. Proc Natl Acad Sci U S A *108*, 15852-15857.
Marques, G., Haerry, T.E., Crotty, M.L., Xue, M., Zhang, B., and O'Connor, M.B. (2003). Retrograde Gbb signaling through the Bmp type 2 receptor wishful thinking regulates systemic FMRFa expression in Drosophila. Development *130*, 5457-5470.
Owusu-Ansah, E., Song, W., and Perrimon, N. (2013). Muscle mitohormesis promotes longevity via systemic repression of insulin signaling. Cell *155*, 699-712.
Palm, W., Sampaio, J.L., Brankatschk, M., Carvalho, M., Mahmoud, A., Shevchenko, A., and Eaton, S. (2012). Lipoproteins in Drosophila melanogaster--assembly, function, and influence on tissue lipid composition. PLoS Genet *8*, e1002828.
Park, Y., Kim, Y.J., and Adams, M.E. (2002). Identification of G protein-coupled receptors for Drosophila PRXamide peptides, CCAP, corazonin, and AKH supports a theory of ligand-receptor coevolution. Proc Natl Acad Sci U S A *99*, 11423-11428.
Plongthongkum, N., Kullawong, N., Panyim, S., and Tirasophon, W. (2007). Ire1 regulated XBP1 mRNA splicing is essential for the unfolded protein response (UPR) in Drosophila melanogaster. Biochem Biophys Res Commun *354*, 789-794.
Rajan, A., and Perrimon, N. (2012). Drosophila cytokine unpaired 2 regulates physiological homeostasis by remotely controlling insulin secretion. Cell *151*, 123-137.
Sheng, L., Zhou, Y., Chen, Z., Ren, D., Cho, K.W., Jiang, L., Shen, H., Sasaki, Y., and Rui, L. (2012). NF-kappaB-inducing kinase (NIK) promotes hyperglycemia and glucose intolerance in obesity by augmenting glucagon action. Nat Med *18*, 943-949.

Siudeja, K., Nassari, S., Gervais, L., Skorski, P., Lameiras, S., Stolfa, D., Zande, M., Bernard, V., Rio Frio, T., and Bardin, A.J. (2015). Frequent Somatic Mutation in Adult Intestinal Stem Cells Drives Neoplasia and Genetic Mosaicism during Aging. Cell Stem Cell *17*, 663-674.
Song, W., Ren, D., Li, W., Jiang, L., Cho, K.W., Huang, P., Fan, C., Song, Y., Liu, Y., and Rui, L. (2010). SH2B regulation of growth, metabolism, and longevity in both insects and mammals. Cell Metab *11*, 427-437.
Song, W., Veenstra, J.A., and Perrimon, N. (2014). Control of lipid metabolism by tachykinin in Drosophila. Cell Rep *9*, 40-47.
Zhu, C.C., Boone, J.Q., Jensen, P.A., Hanna, S., Podemski, L., Locke, J., Doe, C.Q., and O'Connor, M.B. (2008). Drosophila Activin- and the Activin-like product Dawdle function redundantly to regulate proliferation in the larval brain. Development *135*, 513-521.